Fe/Co doped molybdenum diselenide: a promising two-dimensional intermediate-band photovoltaic material

IOP Publishing Nanotechnology
Nanotechnology **26** (2015) 195401 (5pp) doi:10.1088/0957-4484/26/19/195401

Fe/Co doped molybdenum diselenide: a promising two-dimensional intermediate-band photovoltaic material

Jiajia Zhang, Haiyan He and Bicai Pan

Key Laboratory of Strongly-Coupled Quantum Matter Physics, Department of Physics, Hefei National Laboratory for Physical Science at Microscale, University of Science and Technology of China, Hefei, Anhui 230026, People's Republic of China

E-mail: bcpan@ustc.edu.cn

Received 23 December 2014, revised 26 February 2015
Accepted for publication 23 March 2015
Published 21 April 2015

Abstract

An intermediate-band (IB) photovoltaic material is an important candidate in developing the new-generation solar cell. In this paper, we propose that the Fe-doped or the Co-doped $MoSe_2$ just meets the required features in IB photovoltaic materials. Our calculations demonstrate that when the concentration of the doped element reaches 11.11%, the doped $MoSe_2$ shows a high absorptivity for both infrared and visible light, where the photovoltaic efficiency of the doped $MoSe_2$ is as high as 56%, approaching the upper limit of photovoltaic efficiency of IB materials. So, the Fe- or Co-doped $MoSe_2$ is a promising two-dimensional photovoltaic material.

Keywords: $MoSe_2$ nanosheet, solar cell, doping of Fe/Co

(Some figures may appear in colour only in the online journal)

1. Introduction

In the modern photovoltaic (PV) industry, moderate-gap semiconductors such as polycrystalline silicon with the gap of 1.7 eV and CdTe with the gap of 1.5 eV are widely used [1], as they can absorb visible light strongly as well as provide a high output voltage. However, almost 53% of solar radiation is contributed by infrared light (i.e. the photon energy >1.6 eV), which is beyond the photovoltaic ability of both polycrystalline silicon and CdTe. Similarly, many other PV materials also absorb solar radiation in narrow energy ranges. Thus, seeking and designing new materials which can absorb solar radiation in a broad energy region is still an issue.

Following intensive efforts, the intermediate-band (IB) materials have been proposed as promising PV materials [2–8]. For these materials, the intermediate bands are introduced in their forbidden bands, to assist an electron at the valence band to jump to an IB state first and then to a conduction band. Clearly, the IB seems to be a springboard from which to serve the absorption of two photons with energy smaller than the band gap of the host materials. It has been estimated that the intermediate-band solar cell (IBSC) could achieve a PV efficiency of 63%, much larger than the value of 40% of the conventional solar cells [2, 9]. So, the introduced IB significantly improves the PV efficiency of the material [10].

So far, it has been realized that a qualified IB material must meet two critical demands:

(1) The IB should be half-filled so as to serve the two-step jumping of an electron as mentioned above [10];
(2) The IB should have delocalized electronic structures so that the generated holes can be transported freely, overcoming the non-radiative recombination between the electrons and the generated holes [11].

The search for IB materials has made progress in recent years. For instance, it was found that Ti- or V-doped In_2S_3 presented a half-filled intermediate band in the gap region of the host semiconductor [12], where the IB had mainly resulted from the interaction of the doped Ti/V atoms with the host atoms nearby. However, there was no evidence to show whether or not the IB in the Ti/V-doped In_2S_3 is delocalized. Instead, S- or Se-doped Si could induce delocalized states within the band gap when the doping concentration of S or Se exceeds a threshold [13, 14]. However, it is not sure whether

the PV efficiency of such S- or Se-doped Si is improved or not with respect to the pure Si samples.

To the best of our knowledge, most studies on IB materials focus on the bulk materials. In fact, two-dimensional (2D) nanosheets display more desirable features, such as excellent flexibility, inexpensive manufacture, and facile shaping to match a variety of devices. Thus, it is highly expected that 2D nanosheets will be explored as good candidates for IB materials.

$MoSe_2$ nanosheets [15, 16] have been regarded as an attractive material in very recent years. Both Fe and Co have more valence electrons than that of Mo. If Mo in a $MoSe_2$ nanosheet is partly replaced by either Fe or Co, these Fe/Co atoms interact with the host atoms, generating intermediate bands within the band gap. If the IB crosses the Fermi energy level, we will have the expected half-filled IB. In this paper, we carefully examine our expectation above, and find that the doped Fe or Co indeed generates IB states to serve the electron transition excited by the absorbed photons. More interestingly, the Fe/Co-doped $MoSe_2$ nanosheet exhibits an excellent performance in PV, with quantum efficiency of 56% for the absorbing solar radiation.

2. Computational details

Basically, IB states are correlated with the electronic structures arising from the doped atoms in a host material. In the present work, we substitute a Fe (or Co) atom for a Mo atom in two different supercells consisting of $4\times4\times1$ (16 Mo atoms) and $3\times3\times1$ (9 Mo atoms) $MoSe_2$ unit cells, which correspond to dopant concentrations C_M (M = Fe or Co) of 6.25% and 11.11% respectively.

All doped systems are handled at the level of spin–polarized density functional theory (DFT) as implemented in the Vienna *ab initio* Simulation Package (VASP) [17]. The exchange and correlation interaction between electrons are treated by local density approximation (LDA), and the projector-augmented wave (PAW) [18, 19] method with a plane–wave cutoff of 500 eV is adopted. The periodic boundary conditions are applied and a vacuum space of 20 Å is used to avoid the interaction between the sheet and its images. The $4\times4\times1$ and $6\times6\times1$ Monkhorst–Pack K-point grids are used to sample the Brillouin zones of $4\times4\times1$ and $3\times3\times1$ supercells respectively. During the electronic self-consistency loop, the criterion of a 1×10^{-5} eV for the total energy convergence is required. The lattice constants and the internal coordinates of each system are fully optimized until the residual Hellmann–Feynman forces are smaller than 0.01 eV $Å^{-1}$.

3. Results and discussions

Initially, we examine the electronic structures of the pure and the Fe-doped $MoSe_2$. For the pure $MoSe_2$, our computed band gap is about 1.6 eV as shown in figure 1(a), which is consistent with the literature [20, 21]. When the concentration of

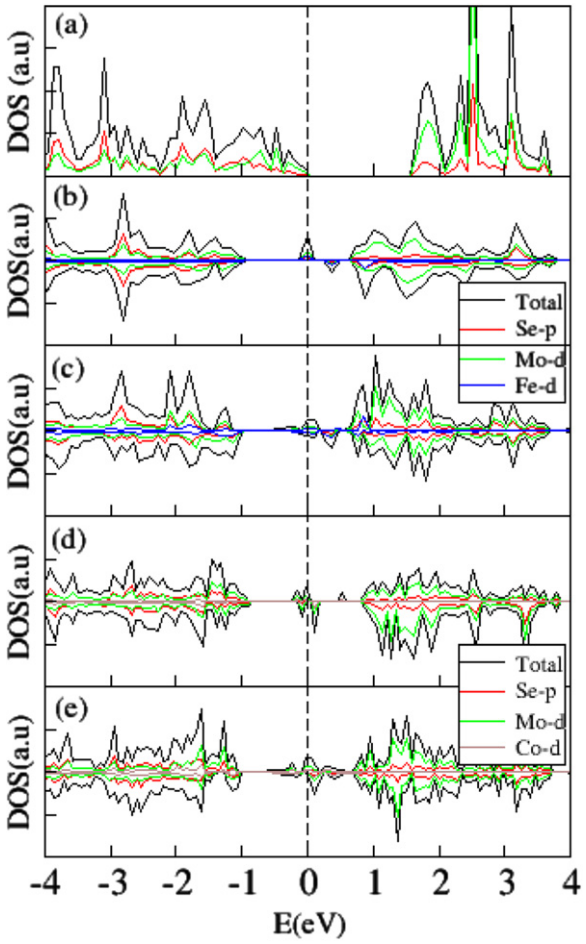

Figure 1. DOS obtained with LDA calculations for pure and Fe/Co-doped $MoSe_2$. (a) Pure $MoSe_2$, (b), (c) $MoSe_2$ with Fe doping concentration of 6.25% and 11.11%, respectively, (d), (e) $MoSe_2$ with Co doping concentration of 6.25% and 11.11%, respectively. The Fermi energy is set to 0.

the doped Fe in the $MoSe_2$ sheet is 6.25%, half-filled impurity states emerge in the gap of $MoSe_2$ (figure 1(b)); when the Fe concentration reaches 11.11%, the impurity states expand in the energy space (figure 1(c)). In this case, the desired IB states actually emerge in the Fe-doped $MoSe_2$ sheet.

Although the Fe-doped $MoSe_2$ possesses the half-filled IB, it is still unclear whether the IB is delocalized or not. Hence, we further examine the distribution of charge density of the IB states in $MoSe_2$ with different concentrations of Fe. As seen in figure 2(a), for the case of $C_{Fe} = 6.25\%$, the charge distribution of the concerned IB states mainly covers the region around the Fe atom and its neighbouring Se and Mo atoms, in which the Fe atom is at the centre site. So, there are a lot of the Fe-central charged regions in the Fe-doped $MoSe_2$, and they do not overlap each other

yet. Thus, the IB states are localized in real space. Such localized charge states expand dramatically for the case of the higher Fe concentrations doping of 11.11%. As shown in figure 2(b), the neighbouring Fe-centred charge states apparently overlap. This indicates that the IB states are delocalized and the system now characterizes the metallic feature, forming channels for the long-distance migration of

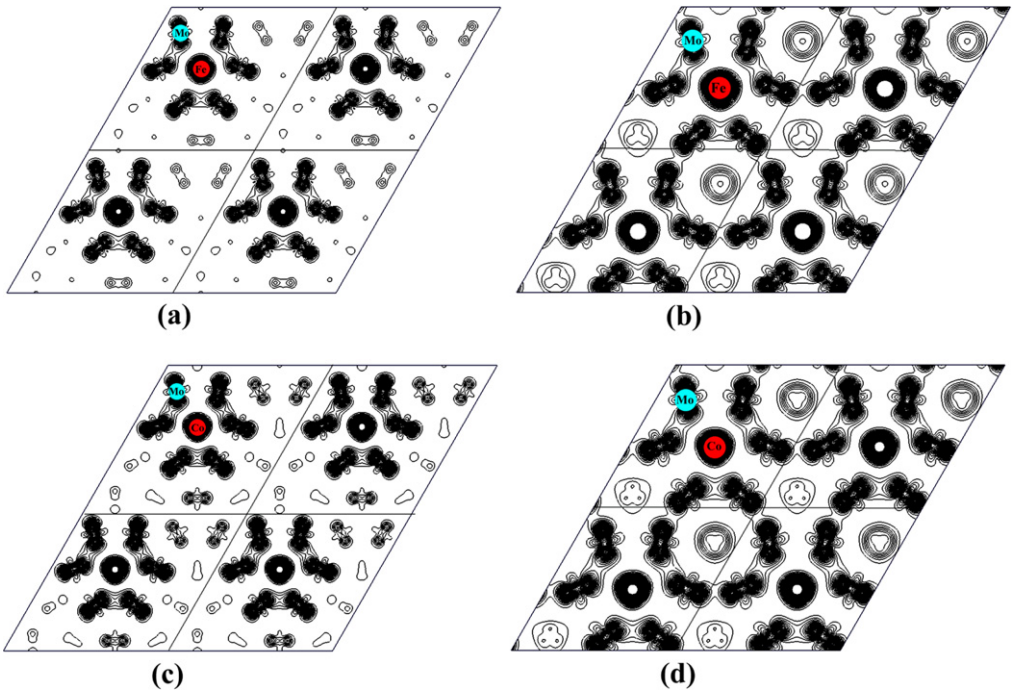

Figure 2. Contour plots of the charge density corresponding to impurity states for (a), (b) $MoSe_2$ with Fe doping concentrations of 6.25% and 11.11%, respectively, and (c), (d) $MoSe_2$ with Co doping concentration of 6.25% and 11.11%, respectively. The planes are for the cross-sectional plane through the Fe/Co and Mo atom. The unit of charge density is $eÅ^{-3}$. The contour levels are from 0 to 0.2 with an interval of 2×10^{-3}.

the excited electrons. Here, the doped Fe is responsible for the typical insulator-to-metal transition observed above. Since the case of $C_{Fe}=11.11\%$ exhibits the delocalized IB states in the Fe-doped $MoSe_2$ sheet, the Fe-doped $MoSe_2$ with $C_{Fe}=11.11\%$ is a potential candidate for PV materials.

We now turn our attention to the capability of optical absorption for such an IB material with $C_{Fe}=11.11\%$. The reflectivity $R(\omega)$ and the absorption coefficient $\alpha(\omega)$ as a function of frequency ω are calculated using the real ($\varepsilon_1(\omega)$) and imaginary parts ($\varepsilon_2(\omega)$) of the dielectric tensors [22]. That is,

$$R(\omega)=\left|\frac{\sqrt{\varepsilon(\omega)}-1}{\sqrt{\varepsilon(\omega)}+1}\right|^2 \quad (1)$$

and

$$\alpha(\omega)=\frac{\omega}{c}\left[2\sqrt{\varepsilon_1^2(\omega)+\varepsilon_2^2(\omega)}-2\varepsilon_1(\omega)\right]^{\frac{1}{2}}. \quad (2)$$

Here, $\varepsilon(\omega)=\varepsilon_1(\omega)+i\varepsilon_2(\omega)$ is the complex dielectric function.

For this system, the computed absorption coefficients are displayed in figure 3(a). Clearly, the photo-absorption region is extended to the whole energy range (0–4 eV) of solar radiation, being much broader than that (1.5–4.0 eV) of the pure system. Essentially, the feature in the photo-absorption does correlate with the transition of electrons between related states. Our calculations indicate that the first absorption peak located at 0.25 eV corresponds to the transition of electrons within the IB, and the absorption spectrum ranging from 0.6 eV to 1.6 eV is mainly attributed to the transition of electrons from valence bands (VB) to IB, followed by the transition from IB to conductive bands (CB). When the energies of the absorbed photons are higher than 1.6 eV, these photon-excited electrons prefer to transition from VB to CB directly. On the whole, as compared to the pure system, the Fe-doped $MoSe_2$ has higher absorptivity for the infrared and the visible light. Besides, since the Fe-doped $MoSe_2$ sheet is optically anisotropic, the dielectric function corresponding to the electric field parallel to the plane of the $MoSe_2$ sheet (notated as the E//plane) should differ from that perpendicular to the plane of the $MoSe_2$ sheet (notated as the E ⊥plane). This is indeed observed in the insets of figures 3(a) and (b), where the absorption intensity corresponding to the case of the E//plane is higher than that of the E ⊥plane.

Usually, a material not only absorbs light, but also reflects light to some extent. The latter definitely also reduces the PV efficiency of the material. So, it is necessary to assess the reflectivity of the $MoSe_2$-based material. According to the results shown in figure 3(a), the pure $MoSe_2$ has a reflectivity of about 20% (blue dashed line) in the whole ranges of the infrared and the visible light, while the Fe-doped $MoSe_2$ just has a higher reflectivity (red dashed line) for the photons whose energies are below 0.5 eV.

Based on the analysis above, we realize that the emergence of IB in Fe-doped $MoSe_2$ can qualitatively improve the absorption for the solar radiation. However, the amplitude of the improved photovoltaic efficiency η is not clear. As we know, the PV efficiency of the material is dependent on several factors. One is the reflection of light from the material. The other one is that the excited electron may transfer from a higher conduction level to the bottom of the conduction band

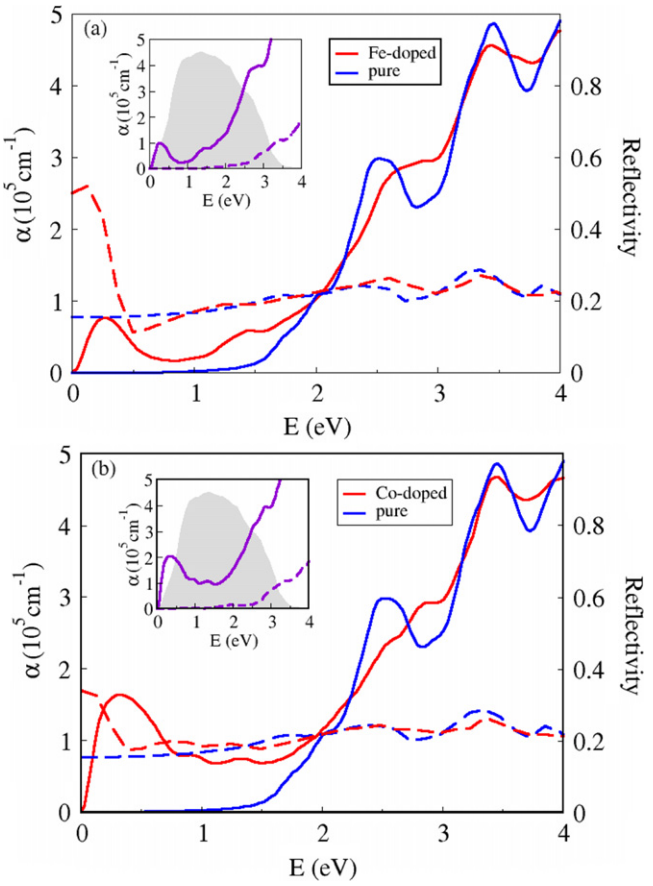

Figure 3. The absorption coefficient (red solid line) and reflectivity (red dashed line) in the infrared and visible spectral range of solar radiation for (a) Fe-doped and (b) Co-doped $MoSe_2$ with doping concentration of 11.11%. As a comparison, the absorption coefficient (blue solid line) and reflectivity (blue dashed line) of pure $MoSe_2$ are also plotted. The insets in (a) and (b) show the absorptivity of the cases of the E//plane (violet solid line) and E⊥plane (violet dashed line) for Fe-doped and Co-doped $MoSe_2$, respectively.

with delivering some energy to the lattice, namely a non-radiation. Similarly, the created holes in the valence bands probably also transfer to the top of the valence band with loss of energy. In consideration of these factors, the PV efficiency η is computed based on the following definition

$$\eta = \frac{\int f(E)A(E)E_g \mathrm{d}E}{\int f(E)E \mathrm{d}E} \tag{3}$$

Here, E is the energy of photon in unit of eV, $f(E)$ represents the relative intensity distribution of the solar radiation, $A(E)$ is the absorptivity, and E_g is the energy difference between the top of VB and the bottom of CB. The integration runs from 0 to 4 eV, covering the whole energy range of the solar radiation. In our calculations, three types of electron transitions in Fe-doped $MoSe_2$ are considered. The first type is the electron transition from IB to IB. In this case, the created electron–hole pairs are within the IB bands, and thus it is easier to have a combination between the electrons and the holes. Because of this, the electron transition within the IB bands does not effectively contribute to the PV efficiency. The second type is the electron transition from VB to IB, and then to CB. This contributes to the absorption in the range from 0.6 eV to 1.6 eV. The third type is the electron transition from VB to CB directly. For the second type above, the transition of an electron correlates the absorption of two photons. So, for this process, we can assume the number of the absorbed photons with energy from 0.6 eV to 1.6 eV is N, and the related number of the excited electrons is $\frac{N}{2}$ accordingly.

In terms of these considerations, the efficiency η of Fe-doped $MoSe_2$ is estimated to be about 55%, being higher than that (40%) of the pure phase. Therefore, the introduction of IB for $MoSe_2$ has significant improvement in PV efficiency.

Extendedly, the Co-doped $MoSe_2$ sheet is also studied. Quite similar to the case of the Fe-doped $MoSe_2$, the Co-doped $MoSe_2$ with Co concentration of 11.11% also displays the half-filled IB states within the original band gap. The basic behaviours in the absorption coefficients and the reflectivity are very close to those of the Fe-doped $MoSe_2$, and the resulting PV efficiency of the Co-doped $MoSe_2$ (56%) is almost the same as that of the Fe-doped $MoSe_2$. Such similarity in the electronic and the PV properties between the Fe-doped and the Co-doped $MoSe_2$ sheets is essentially attributed to the fact that the shell structure and the atom radius of the Fe and Co atoms are very close.

4. Conclusion

In summary, using density functional theory calculations we reveal that the dopants of Fe and Co can induce the half-filled and metallized intermediate-bands in the gap of $MoSe_2$, when the dopant concentration is high enough. More interestingly, their PV efficiencies are predicted to be as high as about 56%, which approaches to the upper limit of efficiency of IB material. So, both the Fe-doped and the Co-doped $MoSe_2$ sheets are potential PV materials.

Acknowledgments

This work is supported by the support of National Basic Research Program of China (2009CB939901). All computations were performed by using the supercomputers of USTC.

References

[1] Henry C H 1980 Limiting efficiencies of ideal single and multiple energy gap terrestrial solar cells *J. Appl. Phys.* **51** 4494
Li H, Wenham S R and Shi Z R 2013 High efficiency perl cells on CZ p-type crystalline silicon using a thermally stable a-Si:H/SiN rear surface passivation stack *Sol. Energy Mater. Sol. Cells* **117** 41
[2] Luque A, Mellor A, Ramiro I, Antolin E, Tobias I and Marti A 2013 Interband absorption of photons by extended states in intermediate band solar cells *Sol. Energy Mater. Sol. Cells* **115** 138

Luque A and Marti A 1997 Increasing the efficiency of ideal solar cells by photon induced transitions at intermediate levels *Phys. Rev. Lett.* **78** 5014

[3] Marti A, Antolin E, Stanley C R, Farmer C D, Lopez N, Diaz P, Canovas E, Linares P G and Luque A 2006 Production of photocurrent due to intermediate-to-conduction-band transitions: a demonstration of a key operating principle of the intermediate-band solar cell *Phys. Rev. Lett.* **97** 247701

[4] Wahnon P and Tablero C 2002 *Ab Initio* electronic structure calculations for metallic intermediate band formation in photovoltaic materials *Phys. Rev.* B **65** 165115

[5] Sanchez K, Aguilera I, Palacios P and Wahnon P 2009 Assessment through first-principles calculations of an intermediate-band photovoltaic material based on ti-implanted silicon: interstitial versus substitutional origin *Phys. Rev.* B **79** 165203

[6] Lopez N, Reichertz L A, Yu K M, Campman K and Walukiewicz W 2011 Engineering the electronic band structure for multiband solar cells *Phys. Rev. Lett.* **106** 028701

[7] Luque A and Marti A 2011 Photovoltaics: towards the intermediate band *Nat. Photonics* **5** 137

[8] Luque A, Marti A and Stanley C 2012 Understanding intermediate-band solar cells *Nat. Photonics* **6** 146

[9] Shockley W and Queisser H J 1961 Detailed balance limit of efficiency of P–N junction solar cells *J. Appl. Phys.* **32** 510

[10] Luque A and Marti A 2001 A metallic intermediate band high efficiency solar cell *Prog. Photovolt. Res. Appl.* **9** 73

[11] Luque A, Marti A, Antolin E and Tablero C 2006 Intermediate bands versus levels in non-radiative recombination *Physica* B **382** 320

[12] Palacios P, Aguilera I, Sanchez K, Conesa J C and Wahnon P 2008 Transition-metal-substituted indium thiospinels as novel intermediate-band materials: prediction and understanding of their electronic properties *Phys. Rev. Lett.* **101** 046403

[13] Winkler M T, Recht D, Sher M J, Said A J, Mazur E and Aziz M J 2011 Insulator-to-metal transition in sulfur-doped silicon *Phys. Rev. Lett.* **106** 178701

[14] Ertekin E, Winkler M T, Recht D, Said A J, Aziz M J, Buonassisi T and Grossman J C 2012 Insulator-to-metal transition in selenium-hyperdoped silicon: observation and origin *Phys. Rev. Lett.* **108** 026401

[15] Coleman J N *et al* 2011 Two-dimensional nanosheets produced by liquid exfoliation of layered materials *Science* **331** 568

[16] Gordon R A, Yang D, Crozier E D, Jiang D T and Frindt R F 2002 Structures of exfoliated single layers of WS_2, MoS_2, and $MoSe_2$ in aqueous suspension *Phys. Rev.* B **65** 125407

[17] Kresse G and Furthmuller J 1996 Efficient iterative schemes for *ab initio* total-energy calculations using a plane-wave basis set *Phys. Rev.* B **54** 11169

[18] Kresse G and Joubert D 1999 From ultrasoft pseudopotentials to the projector augmented-wave method *Phys. Rev.* B **59** 1758

[19] Blöchl P E 1994 Projector augmented-wave method *Phys. Rev.* B **50** 17953

[20] Ding Y, Wang Y L, Ni J, Shi L, Shi S Q and Tang W H 2011 First principles study of structural, vibrational and electronic properties of graphene-like MX_2 (M = Mo, Nb, W, Ta; X = S, Se, Te) monolayers *Physica* B **406** 2254

[21] Wang Q H, Kalantar-Zadeh K, Kis A, Coleman J N and Strano M S 2012 Electronics and optoelectronics of two-dimensional transition metal dichalcogenides *Nat. Nanotechnology* **7** 699

[22] Karazhanov S Z, Ravindran P, Kjekshus A, Fjellvåg H and Svensson B G 2007 Electronic structure and optical properties of ZnX (X = O, S, Se, Te): a density functional study *Phys. Rev.* B **75** 155104